A New Receiver Structure for Asynchronous CDMA: STAR—The Spatio-Temporal Array-Receiver

Sofiène Affes, *Member, IEEE,* and Paul Mermelstein, *Fellow, IEEE*

***Abstract*—We propose a spatio-temporal array-receiver (STAR) for asynchronous code division multiple access (CDMA), using a new space/time structural approach. First, STAR performs blind identification and equalization of the propagation channel from each mobile transmitter. Second, it provides fast and accurate estimates of the number, relative magnitude, and delay of the multipath components. From this space/time separation, STAR reconstructs the identified channel with respect to a partially revealed space/time structure and reduces identification errors by the order of the ratio of the processing gain and the number of paths. Therefore, STAR offers a high potential for increasing capacity, with relatively low computational complexity. Simulations confirm the good multipath acquisition and tracking properties of STAR in the presence of strong interference and fast Doppler.**

***Index Terms*— Array signal processing, blind identification, eigensubspace tracking, equalization and beamforming, localization and tracking, source separation, space–time processing, time-delay synchronization and tracking.**

NOMENCLATURE

a	Scalar.
A	Vector in the time domain.
$\mathbf{A}$	Matrix in the time domain.
$\underline{A}$	Vector reshaping $\mathbf{A}$ column-wise.
$\mathcal{A}$	Vector in the frequency domain.
$\boldsymbol{\mathcal{A}}$	Matrix in the frequency domain.
A^*	Complex conjugate of A.
A^T	Transpose of A.
A^H	Conjugate transpose of A.

Acronyms:

STAR	Spatio-temporal array-receiver.
PCM	Postcorrelation model.
DFI	Decision feedback identification.
STS	Space/time separation.

I. INTRODUCTION

SMART antennas have been recently applied to improve the capacity and the performance of wireless mobile communication systems [1], [2]. They permit the development and the integration of new and powerful array signal processing tools to wireless communications technology. These initial promising results suggest further exploitation of antenna array processing in spread spectrum techniques [3] and motivate the development of new multiuser access methods in asynchronous CDMA [4]–[7]. Most of these techniques (e.g., [4] and [5]) efficiently address processing in space for combining multipath and antenna diversity. However, they use processing in time, for synchronization and sampling, following the classical RAKE structure [3]. As will be seen below, the time-acquisition performance is significantly improved with the new approach.

Indeed, time synchronization and tracking are important issues in cellular CDMA. The performance of the RAKE receiver depends strongly on correct timing. Acquisition of synchronization with a RAKE has generally required hypothesis-testing of likely rough values of a fixed number of multipath time-delays. Once this approximate synchronization has been achieved, the estimates are refined to the required accuracy by means of a closed-loop tracking technique. Therefore, the processing time can be very large, resulting in high complexity since, in the RAKE, both are proportional to the time resolution [3].

Blind multichannel identification, or equalization methods which propose joint space-time processing, offer a good alternative to the RAKE, but usually they have been applied to time division multiple access (TDMA) (see the survey and references in [8]). Recently, some blind multichannel equalization schemes were proposed for code division multiple access (CDMA) (e.g., [9]). These techniques implicitly perform synchronization and array combining by channel equalization in space and time. They process the received signals before correlation, however, and do not exploit effectively the structure of the despread data in CDMA.

Unlike [9], we consider a blind multichannel approach over *the despread data* and develop a block-data formulation, denoted as the postcorrelation model (PCM). The idea of exploiting the data structure after despreading has been already explored in [10] through a simple model for user-localization in spread spectrum techniques. Recently, a more elaborate model of the despread data was developed in [11] in order to implement a blind space-time CDMA receiver, assuming an approximate synchronization of the data. More recently, this model was exploited in [12] to achieve synchronization as well. In this paper, we propose a similar data model which we independently derived previously [13], [14]. This PCM model characterizes the structure of the channel in space and time and can be interpreted as an instantaneous mixture in a one-dimensional spatio-temporal signal subspace. It permits the use of low complexity narrowband array processors and efficient multidimensional signal processing tools.

Manuscript received September 2, 1997; revised March 5, 1998. This work was supported by the Bell Quebec/NORTEL/NSERC Industrial Research Chair in Personal Communications. This paper was presented in part at the IEEE Conferences ICC'97, Montreal, QC, June 1997, and ICUPC'97, San Diego, CA, October 1997.

The authors are with INRS-Telecommunications, Verdun, QC, H3E 1H6, Canada (e-mail: affes@inrs-telecom.uquebec.ca; mermel@inrs-telecom.uquebec.ca).

Publisher Item Identifier S 0733-8716(98)07892-5.

Based upon this PCM model, we propose the use of a spatio-temporal array-receiver (STAR). First, by means of an adaptive subspace-tracking procedure, STAR achieves blind identification and equalization of the channel and implicitly performs integrated and efficient multipath capture and combining in one step. Second, contrary to [9], it exploits the time structure of the identified channel derived from the PCM model and proposes new localization and tracking procedures for estimating the number of paths and their time-delays. Such time characterization was recently considered in [15]–[18] for applications other than CDMA following different approaches. Here, this time characterization achieves a space/time separation (STS) of the identified channel. Channel reconstruction from this space/time decomposition reduces identification errors by the order of the ratio of the processing gain and the number of multipaths and significantly improves the performance of the algorithm.

In analogy with direction of arrival (DOA) estimation techniques, in order to achieve this time characterization of the channel, STAR permits consideration of two multipath time-delay localization options [13]. The first, STAR-SS, performs localization by source-structure analysis. It is very fast and more efficient for slow Doppler. The second, STAR-ES, performs localization by eigenstructure analysis. It is slower and more complex, but more accurate and efficient for fast Doppler. Once localization (i.e., synchronization) has been achieved by either technique, this step is replaced by continuous tracking of the multipath time-delays and their number [14].

STAR provides an attractive and simple receiver structure with relatively low computational complexity. Simulations confirm its effectiveness and its multipath acquisition capability at high interference levels and over a wide range of Doppler.

II. New Block Formulation and Spatio-Temporal Modeling

We consider a cellular CDMA system where each base-station is equipped with a receiving antenna of M sensors. We are mainly interested in the uplink, but we shall show later that STAR is applicable to the downlink as well. The binary phase shift keying (BPSK) bit sequence of the desired user is first differentially encoded at the rate $1/T$, where T is the bit duration [see Fig. 1(a)]. The resulting differential binary phase-shift keying (DBPSK) sequence $b(t)$ is then spread by a periodic personal code $c(t)$ at a rate $1/T_c$, where T_c is the chip pulse duration [see Fig. 1(b)]. The period of $c(t)$ is assumed to be equal to the bit duration T, although the results can be generalized to code periods that are multiples of T. The processing gain is given by $L = T/T_c$. We also assume a multipath fading environment where the number of paths P is unknown and where the time-delay spread $\Delta\tau$ is small compared to T [see Fig. 1(d) and (e)].

At time t, the observation vector received by the antenna array can be written as follows:

$$X(t) = \psi(t)\sum_{p=1}^{P} G_p(t)\varepsilon_p(t)b(t-\tau_p)c(t-\tau_p) + I(t) \quad (1)$$

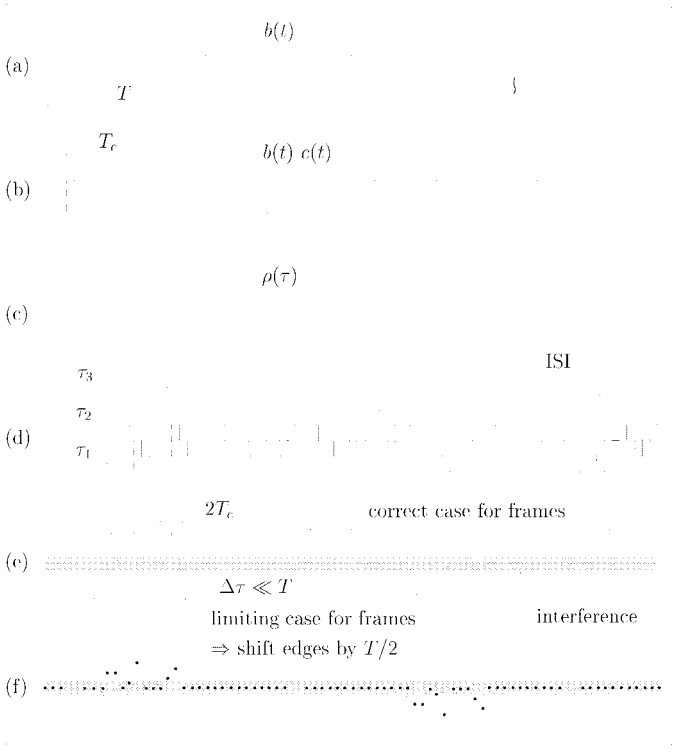

Fig. 1. Data processing steps. (a) DBPSK sequence. (b) Spread sequence (a square pulse is used here for simple illustration). (c) Template of correlation function. (d) Received multipaths. (e) Correlator output containing delayed replicas of the template and interference. (f) Sampling at $1/T_c$ and approximation of the correlation peaks with the main lobes of sinc functions.

where $\tau_p \in [0, T)$ are the propagation time-delays along the P paths, $p = 1, \cdots, P$ and $G_p(t)$ are the propagation vectors with equal norms, their value to be fixed later. $\varepsilon_p^2(t)$ are the fractions along each path [i.e., $\sum_{p=1}^{P} \varepsilon_p^2(t) = 1$] of the total power $\psi^2(t)$ received from the desired user. Estimation of the received power includes the effects of path loss, Rayleigh fading, and shadowing. We assume the time-variations of $G_p(t)$, $\varepsilon_p^2(t)$ and $\psi^2(t)$ to be very slow and locally constant, relative to the bit duration T. The noise term $I(t)$ includes the thermal noise received at the antenna elements as well as the self-, in-cell, and out-cell interference. In order to keep the discussion simple, for the moment we assume that the time-delays are constant. The tracking of time-varying multipath delays is specifically addressed in Section IV.

At successive frames of period T, we now define the postcorrelated observation vector of the frame number n over the time-interval $[0, T)$ by

$$Z_n(t) = \frac{1}{T}\int_0^T X(nT + t + t')c(t')\,dt'. \quad (2)$$

This is actually a general definition of the postcorrelation vector. The classical definition considers $Z_n(t)$ at some particular time-instant $t = \tau_p$, after synchronization by the RAKE receiver (see simplified version of STAR in [19]). This amounts to delaying the postcorrelated data over each path, then sampling it at the bit rate. Here, we consider a continuous stream of the data after despreading and segment it into frames of bit duration T. Since the bit framing is

not aligned across paths received with different delays [see Fig. 1(d)], methods that process the data before correlation (e.g., [9]) result in outputs whose values near the frame boundary reflect contributions from two source bits (as in blind multichannel approaches [8]). In contrast, methods that carry out correlation on separate paths allow location of a frame boundary that is well separated from the correlation peaks, resulting in a composite correlation output in each frame influenced by only a single source bit [see Fig. 1(e)]. As long as the frame boundary lies outside the delay spread interval[1] [see Fig. 1(e)], $Z_n(t)$ of (2) can be developed into

$$Z_n(t) \simeq b(nT)\psi(nT)\sum_{p=1}^{P} G_p(nT)\varepsilon_p(nT)\rho_c(t-\tau_p) + N_n(t) \tag{3}$$

where $\rho_c(t)$ is the correlation function of the chip pulse and $N_n(t)$ is the postcorrelation noise of frame number n. Since the chip pulse is almost time-limited to $[0, T_c]$, its autocorrelation function $\rho_c(t)$ is time-limited to $t \in [-T_c, T_c]$ (i.e., main lobe) and almost null for $|t| \geq T_c$ [see Fig. 1(c)]. Due to its peaky behavior, $\rho_c(t-\tau_p)$ can be viewed as a time-delayed impulse response[2] observed with a frequency resolution $1/T_c$ for an interval $t \in [0, T)$ of the pth path [see Fig. 1(e)].

For each frame, we sample $Z_n(t)$ at the chip rate $1/T_c$ over the interval $t \in [0, T)$ and form the $M \times L$ block data matrix denoted by $\mathbf{Z}_n = [Z_n(0), Z_n(T_c), \cdots, Z_n((L-1)T_c)]$ as the post-correlated observation matrix. Therefore, our approach amounts to sampling the data at the chip rate, as usually made, then stacking it into blocks of length L and of duration T [see Fig. 1(f)]. Oversampling above the chip rate, as in [11] and [12], is not necessary. Notice that, indeed, if the time-delays were integer multiples of the chip duration, then P unknown columns of $\mathbf{Z}_n$ would correspond to the classical postcorrelation vectors, while the remaining columns would correspond to simple interference. In contrast, our method assigns continuous values to the time-delays over the interval $[0, T)$, but the number of paths that can be resolved is still limited by the processing gain L. Each path corresponds to one or, at most, two adjacent columns of $\mathbf{Z}_n$ that can be reasonably approximated by the main lobe of a sinc function sampled at the chip rate[3] [see Fig. 1(f)].

Using (3), $\mathbf{Z}_n$ can be explicitly written as follows:

$$\mathbf{Z}_n = b_n\psi_n\sum_{p=1}^{P} G_{p,n}\varepsilon_{p,n}D_p^T + \mathbf{N}_n = b_n\psi_n\mathbf{G}_n\boldsymbol{\Upsilon}_n\mathbf{D}^T + \mathbf{N}_n \tag{4}$$

where b_n, ψ_n, $G_{p,n}$ and $\varepsilon_{p,n}$ are equal to $b(nT)$, $\psi(nT)$, $G_p(nT)$ and $\varepsilon_p(nT)$, respectively; $\mathbf{G}_n = [G_{1,n}, \cdots, G_{P,n}]$ is the propagation matrix; and $\boldsymbol{\Upsilon}_n = \text{diag}\,\{[\varepsilon_{1,n}, \cdots, \varepsilon_{P,n}]\}$ is the diagonal matrix of power partition over multipaths. Finally, $\mathbf{N}_n = [N_n(0), N_n(T_c), \cdots, N_n((L-1)T_c)]$ is the noise matrix, and $\mathbf{D} = [D_1, \cdots, D_P]$ is the time response matrix, where $D_p = [\rho_c(-\tau_p), \rho_c(T_c-\tau_p), \cdots, \rho_c((L-1)T_c-\tau_p)]^T$ is the time-delay impulse response of path p sampled at $1/T_c$. Its column-by-column fast Fourier transform (FFT) is $\boldsymbol{\mathcal{D}} = [\mathcal{D}_1, \cdots, \mathcal{D}_P]$ and its columns belong to a time manifold, say $\mathbb{\Gamma}$[4]

$$\mathcal{D}_p = \mathcal{F}(\tau_p) = \left[1, e^{-j2\pi\tau_p(1/L)}, \cdots, e^{-j2\pi\tau_p((L-1)/L)}\right]^T \in \mathbb{\Gamma} \quad \text{for } p = 1, \cdots, P. \tag{5}$$

For the sake of simplicity, we may equivalently say that $\mathbf{D}$ or $\boldsymbol{\mathcal{D}}$ belongs to the time manifold $\mathbb{\Gamma}$ without distinction. Later, we shall use this feature to implement the time-delay acquisition step.

We now rewrite (4) in the following compact form:

$$\mathbf{Z}_n = \mathbf{H}_n s_n + \mathbf{N}_n \tag{6}$$

where $\mathbf{H}_n = \mathbf{G}_n\boldsymbol{\Upsilon}_n\mathbf{D}^T = \mathbf{J}_n\mathbf{D}^T$ is the spatio-temporal propagation matrix and $s_n = b_n\psi_n$ is the signal component. Notice here that, while the columns of the time response matrix $\mathbf{D}$ are defined in the manifold $\mathbb{\Gamma}$, the spatial response matrix $\mathbf{J}_n = \mathbf{G}_n\boldsymbol{\Upsilon}_n$ is not modeled[5] and corresponds to the unknown part of the spatio-temporal structure of $\mathbf{H}_n$.

Equation (6) provides a new instantaneous-mixture model at the bit rate where the signal subspace is one-dimensional in the $M \times L$ matrix space. The matrixes $\mathbf{Z}_n$, $\mathbf{H}_n$, and $\mathbf{N}_n$ are transformed into $(M \times L)$-dimensional vectors by arranging their columns as one spatio-temporal column vector to yield

$$\underline{\mathrm{Z}}_n = \underline{\mathrm{H}}_n s_n + \underline{\mathrm{N}}_n \tag{7}$$

where $\underline{\mathrm{Z}}_n$, $\underline{\mathrm{H}}_n$, and $\underline{\mathrm{N}}_n$, respectively, denote the resulting vectors. To avoid the ambiguity due to a multiplicative factor between $\underline{\mathrm{H}}_n$ and s_n, we fix the norm of $\underline{\mathrm{H}}_n$ to $\sqrt{M}$. As mentioned earlier, the norms of the propagation vectors $G_{p,n}$ are implicitly fixed to the same value, say $\sqrt{K_n}$, in such a way that $\|\underline{\mathrm{H}}_n\|^2 = M$. We will explicitly give its expression later.

What is original about the new data block model in (6) or (7) is that the signal component s_n is a scalar and the spatio-temporal signal subspace generated by the space-time propagation vector $\underline{\mathrm{H}}_n$ is one dimensional. It is the correlation step that almost cancels intersymbol interference (ISI) and allows for such a model, contrary to recent blind methods in CDMA (e.g., [9]), which process the data before correlation [see Fig. 1(d) and (e)] following blind multichannel approaches (see the survey in [8]). This model we refer to as the PCM permits any low-complexity narrowband array-processing technique to be

[1] The opposite event could be detected from the localization results. To avoid it, we either run a parallel version or restart the algorithm with the data delayed by $T/2$. The case of a delay spread larger than $T/2$ is under study.

[2] It may be necessary to design pulses whose correlation is very close to a sinc function, but the approximation holds in general.

[3] Intuitively, we approximate the number of resolvable coefficients of an impulse response by fewer sinc functions parameterized by time-delays with continuous values in $[0, T)$.

[4] In [17] and [18], the pulse function which modulates the symbols is included in the time manifold. Similarly, it is the exact correlation function of the chip code $\rho_c(t)$ that should be included here as in [11] and [12], but the approximation made with simple delays is satisfying in the CDMA context. In any case, we avoid the zero-entries problem reported in [18], since no inversion (i.e., deconvolution) is involved in our approach.

[5] We may characterize $\mathbf{G}_n$ in a space manifold parameterized by angles of arrivals as in [16]–[18]. However, a space characterization is often much more restrictive than a time characterization. Besides, it requires perfect antenna calibration and adequate sensor positioning.

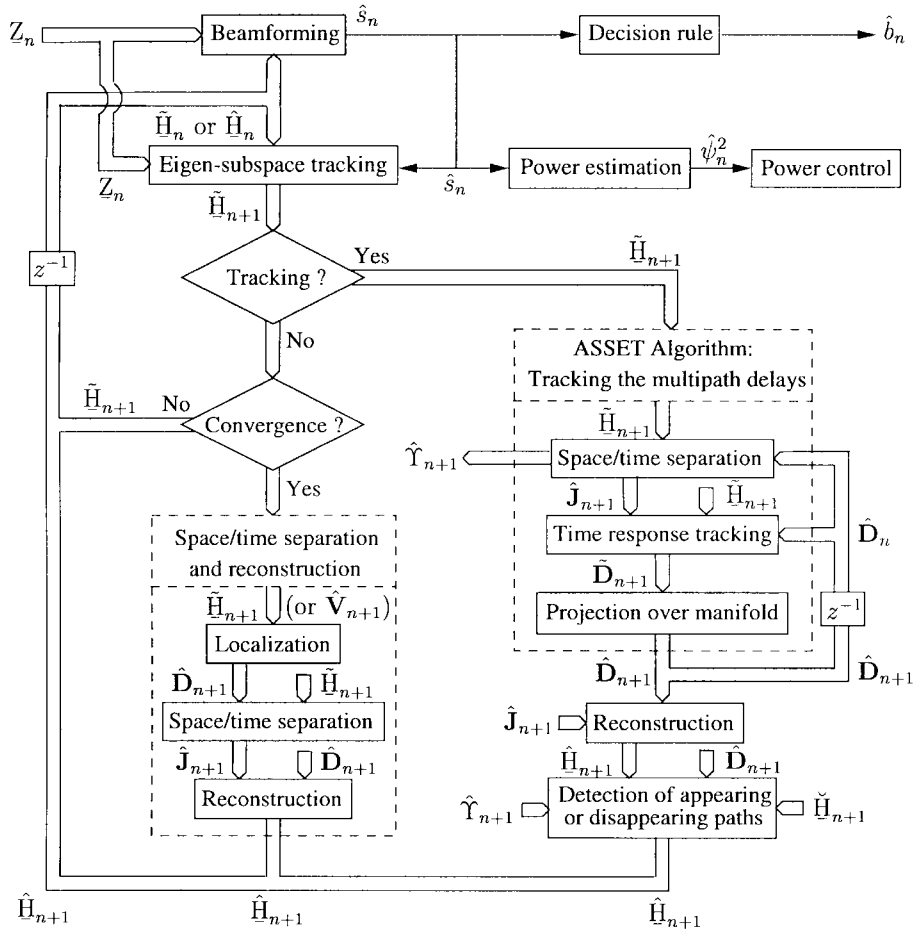

Fig. 2. Block diagram of STAR operations. The eigensubspace tracking procedures of (15) that provide $\hat{\mathbf{V}}_{n+1}$ for localization with STAR-ES and the tracking procedure of (33) that provides $\breve{\underline{H}}_{n+1}$ for the detection of appearing paths are not shown.

used. In particular, either eigensubspace tracking or principal-component analysis methods could be used to identify $\underline{\mathrm{H}}_n$ in a blind approach. Narrowband array beamformers could be used to estimate s_n from such estimates of $\underline{\mathrm{H}}_n$ in a blind space-time-equalization-like step.

Next, using (7), we first propose a spatio-temporal identification and equalization procedure adapted from [19] for simultaneously estimating $\underline{\mathrm{H}}_n$ and s_n, as shown in Fig. 2. Second, using (6), we derive a structural STS and reconstruction of the identified channel after convergence (i.e., $\mathbf{H}_n = \mathbf{J}_n\mathbf{D}^T$). This step captures multipath delays, reduces identification errors by a factor of L/P, and improves the performance of STAR, as shown later by simulations. Finally, the two steps can be integrated for multipath tracking, as explained in Section IV.

III. The Proposed Structure of STAR

A. Spatio-Temporal Identification and Equalization

We first assume that an estimate of $\underline{\mathrm{H}}_n$, say $\tilde{\underline{\mathrm{H}}}_n$, is available at each block iteration n [19]. From this estimate (see Fig. 2), we can extract the signal component s_n by any distortionless beamformer W_n (i.e., $W_n^H\tilde{\underline{\mathrm{H}}}_n = 1$). It is reasonable to assume $\underline{\mathrm{N}}_n$ to be an uncorrelated white noise vector, in which case a delay-sum (DS) beamformer (i.e., $W_n = \tilde{\underline{\mathrm{H}}}_n/M$) is optimal for source extraction [19]. This beamformer achieves a spatio-temporal blind equalization by matched filtering in an $M \times L$ dimensional space and estimates s_n by

$$\hat{s}_n = \mathrm{Real}\Big\{W_n^H\underline{\mathrm{Z}}_n\Big\} = \mathrm{Real}\Big\{\tilde{\underline{\mathrm{H}}}_n^H\underline{\mathrm{Z}}_n/M\Big\} \tag{8}$$

where the Real$\{.\}$ function extracts the real signal component sequence $s_n = \psi_n b_n$ and further reduces the noise by half [19]. The total power received from the desired user is estimated for power control by

$$\hat{\psi}_n^2 = (1-\alpha)\hat{\psi}_{n-1}^2 + \alpha|\hat{s}_n|^2 \tag{9}$$

where $\alpha \ll 1$ is a smoothing factor (see [19] for more details), while the bit sequence $\hat{b}_n$ is estimated from the sign of $\hat{s}_n$. Finally, we track $\underline{\mathrm{H}}_n$ in a blind identification scheme by the following simple and fast least mean square (LMS)-type eigensubspace tracking procedure [19]

$$\tilde{\underline{\mathrm{H}}}_{n+1} = \tilde{\underline{\mathrm{H}}}_n + \mu_n\Big(\underline{\mathrm{Z}}_n - \tilde{\underline{\mathrm{H}}}_n\hat{s}_n\Big)\hat{s}_n^* \tag{10}$$

where μ_n is an adaptation step-size, possibly normalized. Notice that $\hat{b}_n\hat{\psi}_n$ can be used instead of $\hat{s}_n$. This equation converges to $\underline{\mathrm{H}}_n$, with norm $\sqrt{M}$ within a sign ambiguity (i.e., $\tilde{\underline{\mathrm{H}}}_n \simeq \pm\underline{\mathrm{H}}_n$ when $n \to \infty$) [19]. Since b_n is a DBPSK sequence, this ambiguity has no consequences other than changing the signs of $\hat{s}_n$ and $\hat{b}_n$. For the sake of simplicity,

and without loss of generality, we assume in the following that $\tilde{\underline{\mathrm{H}}}_n$ converges to $\underline{\mathrm{H}}_n$.

Other eigensubspace tracking techniques can be used to estimate $\underline{\mathrm{H}}_n$ as well. The identification procedure we proposed in (10), however, is original in that it combines eigensubspace tracking with decision feedback through $\hat{s}_n$ as a reference signal. This decision feedback identification (DFI) feature forces the convergence to $\underline{\mathrm{H}}_n$ within a sign ambiguity. It also achieves the reduction of interference by half, by taking the real part of the beamformer output in (8). This DFI feature increases the capacity by a factor of almost two, as shown in [19]. Other eigensubspace tracking techniques estimate $\underline{\mathrm{H}}_n$ within a phase ambiguity and have no control over it. Thus, they do not achieve this additional gain in capacity.

At this stage, STAR achieves all the required goals, as shown by Fig. 2. It implicitly synchronizes the data through channel equalization without time-delays acquisition, simultaneously estimates the bit sequence, and controls the transmitted power, all at a low order of complexity of $O(ML)$. Additionally, assigning to the identified channel a partially known space/time structure, i.e., $\mathbf{H}_n = \mathbf{J}_n\mathbf{D}^T$ and $\mathbf{D} \in \mathbb{\Gamma}$ to the identified channel significantly reduces identification errors and improves the performance of STAR. This idea which was, to our knowledge, first explored in [20], relies on an algorithm we refer to here as the adaptive source-subspace extraction and tracking (ASSET) technique (see [21] and [22] and related references therein). We next address this point.

B. Structural Space/Time Separation (STS) and Reconstruction

In the following, we propose two time-delay acquisition techniques (i.e., estimation of $\hat{\mathbf{D}} \in \mathbb{\Gamma}$) that can be applied in complementary situations, covering a very wide range of time-variations of the spatial matrix $\mathbf{J}_n$. As explained below (see Fig. 2), these procedures achieve a space/time separation of the spatio-temporal matrix (i.e., estimation of $\hat{\mathbf{J}}_n$) and allow its reconstruction (i.e., $\hat{\mathbf{H}}_n = \hat{\mathbf{J}}_n\hat{\mathbf{D}}^T$ instead of $\tilde{\mathbf{H}}_n$), with a reduction of identification errors by a factor of L/P.

1) STAR-SS—Source-Structure Time-Delay Acquisition Approach: Consider the situation where the time-variations of the spatial matrix $\mathbf{J}_n$ are slow enough, a case applicable to the range of Rayleigh Doppler so far considered in cellular CDMA, so that the spatio-temporal identification by (10) can be made with an acceptable error. Indeed, the time-variations of $\underline{\mathrm{H}}_n$ involve those of $\mathbf{J}_n$, which degrade identification as they increase.

Once convergence of $\tilde{\underline{\mathrm{H}}}_n$ is reached (see Fig. 2), we can redivide it into an $M \times L$ matrix with respect to the PCM model and obtain

$$\tilde{\mathbf{H}}_n^T = \mathbf{D}\mathbf{J}_n^T + \mathbf{E}_n^T \tag{11}$$

where $\mathbf{E}_n^T$, the matrix of identification errors, is considered as a small additive noise matrix. Let us then define the column-by-column FFT of $\tilde{\mathbf{H}}_n^T$ by

$$\tilde{\boldsymbol{\mathcal{H}}}_n = \boldsymbol{\mathcal{D}}J_n^T + \boldsymbol{\mathcal{E}}_n \tag{12}$$

where $\boldsymbol{\mathcal{E}}_n$ denotes the column-by-column FFT of $\mathbf{E}_n^T$. From this equation, the estimation of $\boldsymbol{\mathcal{D}}$ and $\mathbf{J}_n$, which amounts to a space/time-like separation, can be achieved in a way similar to source separation. Other techniques [17], [18] rely on a space-time model of the channel similar to (11), but mainly deal with a 2D localization problem. Here, we give a different interpretation of the channel and address the issue of the STS of its structure, to which we refer as the STS approach.

According to this view, the column vectors of $\tilde{\boldsymbol{\mathcal{H}}}_n$ constitute observation vectors, as if received by L antennas in M parallel spaces. On the other hand, the column vectors of $\mathbf{J}_n^T$ can be seen as signal vectors of P sources that differ from one space to another. However, all these sources propagate in the M different spaces along the same trajectories defined by the common propagation matrix $\boldsymbol{\mathcal{D}}$, where the multipath time-delays $\tau_{p,n}$ correspond to DOA's of plane-wave sources [see (5)]. The time manifold $\mathbb{\Gamma}$ contains $\boldsymbol{\mathcal{D}}$ (or $\mathbf{D}$) and can be viewed as an array manifold. Therefore, any narrowband array processing technique for DOA estimation (i.e., localization, tracking, etc., ...) or for source separation applies by virtue of the PCM model. DOA techniques (see [23] for more details) can be used first to estimate and then to combine the time-delays $\hat{\tau}_{p,n}$ (i.e., $\hat{\boldsymbol{\mathcal{D}}}$ or $\hat{\mathbf{D}}$) over each of the M observation spaces or columns of $\tilde{\boldsymbol{\mathcal{H}}}_n$. Multisource beamforming can be used subsequently to separate the spatial response matrix $\hat{\mathbf{J}}_n^T$ as if it were a signal matrix.

Based on the above analogy, $\mathcal{F}(\tau)^H\tilde{\boldsymbol{\mathcal{H}}}_n\tilde{\boldsymbol{\mathcal{H}}}_n^H\mathcal{F}(\tau)/(ML^2)$ can be viewed as a classical spectrum of DS beamforming averaged over sensors. It measures the average energy of $\mathcal{F}(\tau) \in \mathbb{\Gamma}$ that is present in the M parallel source-subspaces generated by $\tilde{\boldsymbol{\mathcal{H}}}_n$, and its resolution to the chip pulse duration T_c is sufficient for time-delay localization. Hence, we define the localization spectrum of STAR-SS in the frequency domain as

$$\mathcal{S}_{\mathrm{SS}}(\tau) = \frac{1}{1 - \mathcal{F}(\tau)^H\tilde{\boldsymbol{\mathcal{H}}}_n\tilde{\boldsymbol{\mathcal{H}}}_n^H\mathcal{F}(\tau)/ML^2}. \tag{13}$$

This spectrum reveals P peaks at the time-delay locations, from which estimates of the number of paths $\hat{P}$ and their time-delays $\hat{\tau}_1, \cdots, \hat{\tau}_{\hat{P}}$ can be obtained.

By analogy to a reference algorithm for source localization, MUSIC [24], [25], we avoid the prohibitive search over the time-delay locations in $[0, T)$ and propose a solution that is similar to Root-MUSIC [26]. We define the following $(2L-2)$-degree polynomial

$$\mathcal{P}_{\mathrm{SS}}(z) = 1 - \mathcal{F}(\tau)^H\tilde{\boldsymbol{\mathcal{H}}}_n\tilde{\boldsymbol{\mathcal{H}}}_n^H\mathcal{F}(\tau)/ML^2 \tag{14}$$

where $z = e^{-j2\pi\frac{\tau}{T}}$. Let $\hat{z}_1, \cdots, \hat{z}_{L-1}$ denote the $L-1$ roots inside the unit circle of the equation $\mathcal{P}_{\mathrm{SS}}(z) = 0$. Then $\mathcal{P}_{\mathrm{SS}}(\hat{z}_1/|\hat{z}_1|), \cdots, \mathcal{P}_{\mathrm{SS}}(\hat{z}_{L-1}/|\hat{z}_{L-1}|)$ reveal the extrema of the spectrum $\mathcal{S}_{\mathrm{SS}}(\tau)$ and give $\hat{P}$ and $\hat{\tau}_1, \cdots, \hat{\tau}_{\hat{P}}$ if the delays are assigned in order of decreasing spectrum magnitude. Then $\hat{\mathbf{D}}$ is the column-by-column inverse FFT of $\hat{\boldsymbol{\mathcal{D}}} = [\mathcal{F}(\hat{\tau}_1), \cdots, \mathcal{F}(\hat{\tau}_{\hat{P}})]$.

2) STAR-ES—Eigenstructure Time-Delay Acquisition Approach: Consider now the situation in which the time-variations of $\mathbf{J}_n$ are very fast, so that the spatio-temporal identification errors become very high. In this case we apply an eigenstructure-based approach to the postcorrelated

observation matrix $\mathbf{Z}_n^T$ in (6), instead of $\tilde{\mathbf{H}}_n^T$ in (11). Here, we exploit new adaptations of MUSIC [24], [25] and of Root-MUSIC [26] for a better illustration, but other high resolution techniques, such as ESPRIT [29] or the ML approach [27], [28], can be used as well (see [15]–[18]).

In this approach, it is reasonable to assume uncorrelated multipaths at the same antenna. Using the same analogy developed earlier, the column vectors of $\mathbf{J}_n^T$ can again be regarded as signal vectors of P uncorrelated sources in M parallel spaces, propagating from one space to another along the same trajectories, but with different statistics. As the time-variations of $\mathbf{J}_n$ increase (e.g., very fast Doppler), the variations of the short-term statistics gathered locally during short observation time-intervals decrease and the source signals (i.e., multipath components) become more stationary over larger time-intervals. Note that (10) is still necessary for power control. Contrary to STAR-SS, faster time-variations of $\mathbf{J}_n$ speed up the convergence, since STAR-ES involves the statistics of $\mathbf{J}_n$, rather than its instantaneous realizations.

Over the mth column vector of $\mathbf{Z}_n^T$, denoted by $Z_{m,n}$, define now the signal eigensubspace by the $L \times P$ eigenmatrix $\mathbf{U}_m$, corresponding to the P largest eigenvalues of the correlation matrix R_{Z_m} of $Z_{m,n}$. Then for $m = 1, \cdots, M$ and $p = 1, \cdots, P$ we have $\mathcal{F}(\tau_p)^H \boldsymbol{\mathcal{U}}_m \boldsymbol{\mathcal{U}}_m^H \mathcal{F}(\tau_p)/L^2 = 1$, where $\boldsymbol{\mathcal{U}}_m$ denotes the column-by-column FFT of $\mathbf{U}_m$. Similar to the previous approach, we shall use this high-resolution feature to provide a localization spectrum and its root solutions, but first we need to estimate the signal eigenmatrices $\mathbf{U}_m$.

We propose an adaptive eigensubspace tracking technique similar to [21], which can be seen as an asymptotic version of [30] after convergence, but other algorithms can be used as well[6] (see references in [30]). Remember that we need an initial estimate of the dimension P of the signal eigensubspace. To show the robustness of STAR-ES with respect to this initial rank estimation, we define here $P_{\max} \ll L$ as the maximum number of resolvable paths that may be present at the same time (i.e., $P < P_{\max}$) and track the $L \times P_{\max}$ eigenmatrix $\hat{\mathbf{U}}_{m,n}$ for $m = 1, \cdots, M$ by

$$\hat{\mathbf{U}}_{m,n+1} = \hat{\mathbf{U}}_{m,n} + \eta_{m,n}(Z_{m,n} - \hat{\mathbf{U}}_{m,n} Y_{m,n}) Y_{m,n}^H \quad (15)$$

where $\eta_{m,n}$ is an adaptation step-size, possibly normalized, and $Y_{m,n} = \hat{\mathbf{U}}_{m,n}^H Z_{m,n}$. This equation is a simple approximation of an LMS version of [30] and behaves nearly as well as the exact solution. It converges to the $L \times P_{\max}$ eigenmatrix of R_{Z_m} corresponding to its $P_{\max}$ largest eigenvalues[7] such that $\hat{\mathbf{U}}_{m,n}^H \hat{\mathbf{U}}_{m,n} = I_{P_{\max}}$.

Once convergence is reached (see Fig. 2), we define the localization spectrum of STAR-ES by

$$\mathcal{S}_{\mathrm{ES}}(\tau) = \frac{1}{1 - \mathcal{F}(\tau)^H \hat{\boldsymbol{\mathcal{V}}}_n \hat{\boldsymbol{\mathcal{V}}}_n^H \mathcal{F}(\tau)/ML^2} \quad (16)$$

where the $L \times (MP_{\max})$ matrix $\hat{\boldsymbol{\mathcal{V}}}_n$ is the column-by-column FFT[8] of $\hat{\mathbf{V}}_n = [\hat{\mathbf{U}}_{1,n}, \cdots, \hat{\mathbf{U}}_{M,n}]$. Its root solutions are given in a way similar to STAR-SS using the following polynomial:

$$\mathcal{P}_{\mathrm{ES}}(z) = 1 - \mathcal{F}(\tau)^H \hat{\boldsymbol{\mathcal{V}}}_n \hat{\boldsymbol{\mathcal{V}}}_n^H \mathcal{F}(\tau)/ML^2 \quad (17)$$

and provide $\hat{P}$ and $\hat{\tau}_1, \cdots, \hat{\tau}_{\hat{P}}$ as well as $\hat{\mathbf{D}}$. $\hat{\boldsymbol{\mathcal{V}}}_n$ contains $(P_{\max} - P)$-dimensional noise eigensubspaces. The performance in localization decreases as $(P_{\max} - P)$ increases, but still remains acceptable in practical situations.

3) Spatio-Temporal Separation and Reconstruction: As discussed at the beginning of Section III-B1, once $\hat{\mathbf{D}}$ is estimated, we resort to the STS approach and separate $\hat{\mathbf{J}}_n^T$ as a signal-like matrix by multisource beamforming [21] and compute its constituent elements $\hat{\mathbf{G}}_n$ and $\hat{\boldsymbol{\Upsilon}}_n$ as follows:

$$\hat{\mathbf{J}}_n^T = \left[\hat{J}_{1,n}, \cdots, \hat{J}_{\hat{P},n}\right]^T = \left(\hat{\mathbf{D}}^T \hat{\mathbf{D}}\right)^{-1} \hat{\mathbf{D}}^T \tilde{\mathbf{H}}_n^T \quad (18)$$

$$\hat{\mathbf{G}}_n = ||\hat{\mathbf{J}}_n||_F \left[\frac{\hat{J}_{1,n}}{||\hat{J}_{1,n}||}, \cdots, \frac{\hat{J}_{\hat{P},n}}{||\hat{J}_{\hat{P},n}||}\right] \quad (19)$$

$$\hat{\boldsymbol{\Upsilon}}_n = \mathrm{diag}\left\{\left[\frac{||\hat{J}_{1,n}||}{||\hat{\mathbf{J}}_n||_F}, \cdots, \frac{||\hat{J}_{\hat{P},n}||}{||\hat{\mathbf{J}}_n||_F}\right]\right\} \quad (20)$$

where $||.||_F$ denotes the Frobenius norm of a matrix. Finally, we reconstruct the spatio-temporal propagation matrix $\hat{\mathbf{H}}_n$, or equivalently $\underline{\hat{\mathbf{H}}}_n$ (see Fig. 2), with respect to the spatio-temporal structure of the channel in (4) by

$$\hat{\mathbf{H}}_n = \hat{\mathbf{G}}_n \hat{\boldsymbol{\Upsilon}}_n \hat{\mathbf{D}}^T = \hat{\mathbf{J}}_n \hat{\mathbf{D}}^T. \quad (21)$$

The norms of the propagation vectors $\sqrt{K_n}$ are equal to $||\hat{\mathbf{J}}_n||_F = (\sum_{p=1}^{\hat{P}} ||\hat{J}_{p,n}||^2)^{1/2}$ such that $||\hat{\mathbf{H}}_n||_F = \sqrt{M}$. Using (18) and (11) and assuming $\hat{\mathbf{D}} \simeq \mathbf{D}$, we can write

$$\hat{\mathbf{H}}_n = \mathbf{H}_n + \mathbf{E}_n \hat{\mathbf{D}} \left(\hat{\mathbf{D}}^T \hat{\mathbf{D}}\right)^{-1} \hat{\mathbf{D}}^T. \quad (22)$$

The reconstruction projects the matrix of identification errors $\mathbf{E}_n$ onto the source-subspace defined by $\hat{\mathbf{D}}$ and reduces its energy by a factor of L/P. It significantly improves the performance of STAR, as shown by the simulations of Section V.

IV. Tracking the Number of Multipaths and their Delays

Up to this point we have considered constant multipath time-delays for the sake of simplicity. In the following, we allow them to vary with time and denote them by $\tau_{1,n}, \cdots, \tau_{P,n}$. We also assume that $\hat{\tau}_{1,n}, \cdots, \hat{\tau}_{\hat{P},n}$ as well as $\hat{P}$ have been previously estimated by either STAR-SS or STAR-ES. In order to maintain the gain of L/P in identification errors achieved in Section III-B after localization, we need to update the underlying space/time separation and reconstruction of the channel to the time-variations of $\tau_{1,n}, \cdots, \tau_{P,n}$. At each iteration, we therefore reestimate $\hat{\mathbf{H}}_n = \hat{\mathbf{J}}_n \hat{\mathbf{D}}_n^T$ from $\tilde{\mathbf{H}}_n$.

The spatio-temporal identification and equalization of the channel introduced in Section III-A can be modified as follows

[6] The use of these techniques is justified by the fact that each column of the noise matrix $\mathbf{N}_n^T$ can often be approximated as an uncorrelated white noise vector.

[7] If R_{Z_m} can be assumed identical for $m = 1, \cdots, M$ (e.g., ultra high Doppler), we can take the average of (15) over sensors in a joint eigensubspace tracking scheme.

[8] $\hat{\mathcal{V}}_n$ could be directly estimated using (15) in the frequency domain.

(see Fig. 2). The LMS-type identification procedure of (10) is replaced after convergence and initial localization by

$$\underline{\tilde{\mathrm{H}}}_{n+1} = \underline{\hat{\mathrm{H}}}_n + \mu_n(\underline{\mathrm{Z}}_n - \underline{\hat{\mathrm{H}}}_n\hat{s}_n)\hat{s}_n^* \tag{23}$$

while the equalization step by space/time narrowband beamforming of (8) is replaced by

$$\hat{s}_n = \mathrm{Real}\Big\{\underline{\hat{\mathrm{H}}}_n^H \underline{\mathrm{Z}}_n/M\Big\}. \tag{24}$$

Compared to the previous formulations, both equations take advantage of a new and permanent gain in identification errors over $\underline{\hat{\mathrm{H}}}_n$ by a factor of L/P. They further improve the performance of the algorithm in terms of time-acquisition and reception by incorporating DFI features over both the signal and the channel (see discussion in Section III-A).

To estimate $\underline{\hat{\mathrm{H}}}_{n+1}$ from $\underline{\tilde{\mathrm{H}}}_{n+1}$ of (24), we could apply at each iteration the time-delays localization procedures described earlier STAR-SS or STAR-ES. These procedures, however, are computationally excessively complex relative to the identification and equalization step. It is simpler to apply them in a single iteration, in order to provide initial estimates of the multipath time-delays. Once an initial time-acquisition is made, either localization procedure can be replaced by a time-delays tracking algorithm.

Indeed, we resort again to the STS approach and to the same analogy established earlier (11) with DOA estimation problems. We consider here the application of low-complexity DOA tracking methods for the tracking of the number of multipaths and their time-delays. We apply the ASSET algorithm [21] to STAR, because it is very simple to implement and it optimally exploits the space manifold structure for DOA tracking (see a comparative evaluation with promising methods in [31]). As explained next (see Fig. 2), we adapt it here to time-delays tracking in a time-manifold,[9] in order to maintain a low computational cost for STAR without assuming time-invariant localization.

A. Tracking the Multipath Delays

Using the estimate $\hat{\mathbf{D}}_n$ as an approximation of $\mathbf{D}_{n+1}$ [21], we modify (18) and compute the signal-like matrix $\hat{\mathbf{J}}_{n+1}^T$ as the output of a multidimensional DS (delay-sum) beamformer

$$\hat{\mathbf{J}}_{n+1}^T = \Big[\hat{J}_{1,\,n+1},\,\cdots,\,\hat{J}_{\hat{P},\,n+1}\Big]^T = \Big(\hat{\mathbf{D}}_n^T\hat{\mathbf{D}}_n\Big)^{-1}\hat{\mathbf{D}}_n^T\tilde{\mathbf{H}}_{n+1}^T. \tag{25}$$

This beamformer is optimal if $\mathbf{E}_{n+1}^T$ in (11) is an uncorrelated white noise matrix. In most cases, such an assumption is reasonable. Otherwise, we may apply the optimal beamformer proposed in [22]. The computational complexity in (25) is of $O(LP^2 + P^3 + MPL + MP^2)$, but it can be reduced to $O[MP(L+1)]$ with the iterative implementation of [22]. From (25), the estimation of $\hat{\mathbf{G}}_{n+1}$ and $\hat{\boldsymbol{\Upsilon}}_{n+1}$ follows by (19) and (20).

We now update the time response matrix $\hat{\mathbf{D}}_n$ in a subspace-tracking equation similar to (10). Although a single observation space is sufficient (i.e., $M = 1$), the combination of the estimates over the M spaces (i.e., exploiting antenna diversity) improves the tracking performance. Taking the average, the tracking equation can be stated in the following compact form:

$$\tilde{\mathbf{D}}_{n+1} = \hat{\mathbf{D}}_n + \frac{\xi_n}{M}\Big(\tilde{\mathbf{H}}_{n+1}^T - \hat{\mathbf{D}}_n\hat{\mathbf{J}}_{n+1}^T\Big)\hat{\mathbf{J}}_{n+1}^* \tag{26}$$

where ξ_n is an adaptation step-size, possibly normalized. The associated computational complexity is $O[(M+1)PL]$.

Note that if $\tilde{\mathbf{H}}_{n+1}^T$ in (26) is replaced by $\mathbf{Z}_n^T$, we obtain the exact expression of the ASSET algorithm in [21], averaged over sensors. Here, we have the advantage of reducing the noise present in $\mathbf{Z}_n^T$ to simple identification errors in $\tilde{\mathbf{H}}_{n+1}^T$ [see (11)]. Thus, (26) allows for multipath tracking at a higher interference level and more mobile transmitters can be accommodated.

We now define $\tilde{\boldsymbol{\mathcal{D}}}_{n+1}$, the column-by-column FFT of $\tilde{\mathbf{D}}_{n+1}$, and constrain its column vectors $\tilde{\mathcal{D}}_{p,\,n+1}$ to lie in $\mathbb{\Gamma}$ for $p = 1, \cdots, \hat{P}$, as in [20] and [21]. This is done with the aid of linear regressions of the phase variations between the L components of $\tilde{\mathcal{D}}_{p,\,n+1}$ and $\hat{\mathcal{D}}_{p,\,n}$ over the L frequency bins $0, 1, \cdots, L-1$. If we define these variations for $l = 1, \cdots, L$ and for $p = 1, \cdots, \hat{P}$ by

$$\delta\hat{\varphi}_{p,\,l,\,n+1} = \mathrm{Im}\Big\{\log\Big(\tilde{\mathcal{D}}_{p,\,l,\,n+1}^*\hat{\mathcal{D}}_{p,\,l,\,n}\Big)\Big\} \tag{27}$$

then $\hat{\tau}_{p,\,n+1}$, the slopes of the linear regressions, and $\hat{\mathcal{D}}_{p,\,n+1} \in \mathbb{\Gamma}$, the vectors of delay transforms, are given in (28) and (29) shown at the bottom of the page where $\mathrm{Im}\{.\}$ in (27) denotes the imaginary part of a complex number (see [20] and [21] for more details). The impulse response matrix $\hat{\mathbf{D}}_{n+1}$ is estimated[10] in the time domain as the column-by-column inverse FFT of

$$\hat{\boldsymbol{\mathcal{D}}}_{n+1} = \Big[\hat{\mathcal{D}}_{1,\,n+1},\,\cdots,\,\hat{\mathcal{D}}_{\hat{P},\,n+1}\Big].$$

The complexity of this step is $O[P(L + \log L + 1)]$.

[9] We may characterize $\hat{\mathbf{G}}_n$ in a space manifold, if assumed as in [16]–[18], using the ASSET technique [21].

[10] It is more accurate to directly define the columns $\hat{D}_{p,\,n+1}$ of $\hat{\mathbf{D}}_{n+1}$ as replicas of $\rho_c(t)$, delayed by $\hat{\tau}_{p,\,n+1}$, and sampled at the chip rate. It is even advantageous to set their elements to zero outside the main lobe of $\rho_c(t)$ to discard low SNR samples and select multipath fingers in a RAKE-like fashion [19]. We follow here a general approach that is independent of the exact pulse waveform.

$$\hat{\tau}_{p,\,n+1} = \hat{\tau}_{p,\,n} + \frac{L}{2\pi} \times \left\{ \frac{(L-1)\displaystyle\sum_{l=1}^{L}(l-1)\delta\hat{\varphi}_{p,\,l,\,n+1} - \sum_{k=1}^{L}(k-1)\sum_{l=1}^{L}\delta\hat{\varphi}_{p,\,l,\,n+1}}{(L-1)\displaystyle\sum_{l=1}^{L}(l-1)^2 - \left(\sum_{k=1}^{L}(k-1)\right)^2} \right\} \tag{28}$$

$$\hat{\mathcal{D}}_{p,\,n+1} = \mathcal{F}(\hat{\tau}_{p,\,n+1}) = \Big[1,\, e^{-j2\pi\hat{\tau}_{p,\,n+1}(1/L)},\,\cdots,\, e^{-j2\pi\hat{\tau}_{p,\,n+1}(L-1/L)}\Big]^T \tag{29}$$

We find that this structure fitting step provides robustness to correlated sources and colored noise when applied to DOA tracking [20]–[22]. Similarly, by virtue of including this feature in (28), STAR allows multipath tracking in the presence of colored interference (i.e., near–far resistance) and correlated multipath. Furthermore, an optimal beamformer for the extraction of correlated sources in colored noise was proposed in [22]. A similar beamformer can be implemented in STAR in order to allow for optimal reception in correlated multipath and colored interference in addition to robustness. These issues will be addressed and reported in a later publication.

We finally reconstruct the spatio-temporal response matrix as $\hat{\mathbf{H}}_{n+1} = \hat{\mathbf{J}}_{n+1}\hat{\mathbf{D}}_{n+1}^T$ (see Fig. 2) such that $\|\hat{\mathbf{H}}_{n+1}\|_F = \sqrt{M}$. The computational complexity of this step is of $O[MP(L+1)]$. The total computational complexity required for STAR for multipath tracking is of $O(MPL+ML+PL+P\log L+MP+P)$, with a dominant term of $O(MPL)$.

We can further reduce the complexity of multipath tracking after localization for large values of the processing gain by truncating the data block $\mathbf{Z}_n$ to its $L' < L$ columns that cover the time-delay spread with a sufficient margin for the tracking [i.e., the dominant term of complexity reduces to $O(MPL')$]. Notice also that the above-noted formulation of STAR holds in the limiting case where the number of antennas M is one. Hence, it can be applied to the downlink without a pilot signal or a training sequence.

B. Tracking the Number of Paths

Now that we have established an adaptive procedure for tracking the multipath delays, we consider tracking their number $\hat{P}$, since P may change with time due to paths appearing and disappearing. The strategy we propose relies on the observation in time of energy-based detection criteria proposed in [21] for DOA tracking.

1) The Case of Vanishing Paths: The matrix $\hat{\mathbf{\Upsilon}}_n = \text{diag}\,\{[\hat{\varepsilon}_{1,n}, \cdots, \hat{\varepsilon}_{\hat{P},n}]\}$ of power partition is useful for the detection of vanishing paths. We decide that the pth path has vanished at block iteration n_d if then, and for a number of previous block iterations $n_v - 1$, its power $\hat{\varepsilon}_{p,n}^2$ is constantly below a minimum threshold $\varepsilon_{\min}^2$, i.e.,

$$\hat{\varepsilon}_{p,n}^2 < \varepsilon_{\min}^2 \qquad \text{for } n \in \{n_d - n_v + 1, \cdots, n_d\}. \tag{30}$$

Instead of evaluating this condition over n_v block iterations, we may smooth the elements of $\hat{\mathbf{\Upsilon}}_n$ to introduce a forgetting factor. Both techniques can be combined, if necessary, to avoid false detections. When the above condition is satisfied, we eliminate the pth path and the corresponding estimates, decrement $\hat{P}$ by 1 (i.e., $\hat{P} = \hat{P} - 1$) and update the parameters of the algorithm.

2) The Case of Merging Paths: Another case where the number of paths $\hat{P}$ should be decremented corresponds to the situation when two time-delays get very close and their paths appear to merge into a single one for more than say n_m block iterations. Although this case is unlikely to happen in practice, its absence guarantees a full column-rank condition of $\hat{\mathbf{D}}_n$ and provides for better stability of the algorithm. This situation can be identified at the block iteration n_d for the pth and kth merging paths by the following condition:

$$|\hat{\tau}_{p,n} - \hat{\tau}_{k,n}| < T_c \text{ for } n \in \{n_d - n_m + 1, \cdots, n_d\}. \tag{31}$$

In this case, we eliminate either path, decrement $\hat{P}$ by 1 (i.e., $\hat{P} = \hat{P} - 1$) and update the parameters of the algorithm. Contrary to DOA tracking, no data association is required when the two merged paths split again after less than n_m iterations as if the path-delays had crossed, since they both belong to the same source.

3) The Case of Newly Appearing Paths: We now study the case when a new path appears. Such an event would involve an identification error on the spatio-temporal response matrix $\mathbf{H}_n$, denoted by $\delta\mathbf{H}_n = \varepsilon_{P+1,n}G_{P+1,n}D_{P+1,n}^T$, whose energy can be compared to a maximum threshold for the detection. This error $\delta\hat{\mathbf{H}}_n$ can be estimated in two ways. We can define the noise estimate $\hat{\mathbf{N}}_n = \mathbf{Z}_n - \hat{\mathbf{H}}_n\hat{s}_n$ and directly identify the error in a LMS-type tracking equation similar to (10) as follows:

$$\delta\underline{\hat{\mathbf{H}}}_{n+1} = \delta\underline{\hat{\mathbf{H}}}_n + \zeta_n\left(\underline{\hat{\mathbf{N}}}_n - \delta\underline{\hat{\mathbf{H}}}_n\hat{s}_n\right)\hat{s}_n^* \tag{32}$$

where ζ_n is an adaptation step-size and where $\delta\underline{\hat{\mathbf{H}}}_n$ and $\underline{\hat{\mathbf{N}}}_n$ are the $M \times L$ vectors resulting from the aligned columns of $\hat{\mathbf{H}}_n$ and $\hat{\mathbf{N}}_n$, respectively. With respect to the sequence $\hat{s}_n$ already estimated in (8), this equation is based on an almost exact LMS implementation. We can also identify an unconstrained estimate of the spatio-temporal response matrix, say $\breve{\mathbf{H}}_n$, in another almost exact LMS tracking equation given by

$$\underline{\breve{\mathbf{H}}}_{n+1} = \underline{\breve{\mathbf{H}}}_n + \zeta_n\left(\underline{\mathbf{Z}}_n - \underline{\breve{\mathbf{H}}}_n\hat{s}_n\right)\hat{s}_n^* \tag{33}$$

where $\underline{\breve{\mathbf{H}}}_n$ is the $M \times L$ vector resulting from the aligned columns of $\breve{\mathbf{H}}_n$. This estimate, without the structure fitting constraint in the time manifold $\mathbb{\Gamma}$, tracks all the spatio-temporal components of $\mathbf{H}_n$, including the unresolvable paths. Here, $\delta\hat{\mathbf{H}}_n = \breve{\mathbf{H}}_n - \hat{\mathbf{H}}_n$ is an alternative estimator of the required error. Note that $\hat{b}_n$ can be used instead of $\hat{s}_n$ in (32) and (33) with some appropriate modifications, in order to avoid the effect of time-fluctuations in the power of $\hat{\psi}_n^2$ [see (9)].

Given an estimate $\delta\hat{\mathbf{H}}_n$ of the identification error, we may decide that a new path has appeared at block iteration n_d if, after a given number of block iterations n_a, the relative distortion over $\hat{\mathbf{H}}_n$ given by $\|\delta\hat{\mathbf{H}}_n\|_F^2/\|\hat{\mathbf{H}}_n\|_F^2$ consistently exceeds a maximum threshold, say $\delta_{\max}^2$

$$\frac{\|\delta\hat{\mathbf{H}}_n\|_F^2}{M} > \delta_{\max}^2 \qquad \text{for } n \in \{n_d - n_a + 1, \cdots, n_d\}. \tag{34}$$

Again, a smoothing of the distortion instead of (34), or a combination of both, can be used to avoid false detections. Whenever we detect an excessive identification error, we can apply the localization procedures STAR-SS or STAR-ES to reestimate $\hat{P}$ and the time-delays $\hat{\tau}_{p,n}$ for $p = 1, \cdots, \hat{P}$ and update the parameters of the algorithm.

All the steps of the algorithm described in the current and previous sections are finally illustrated by the block diagram of STAR operations in Fig. 2.

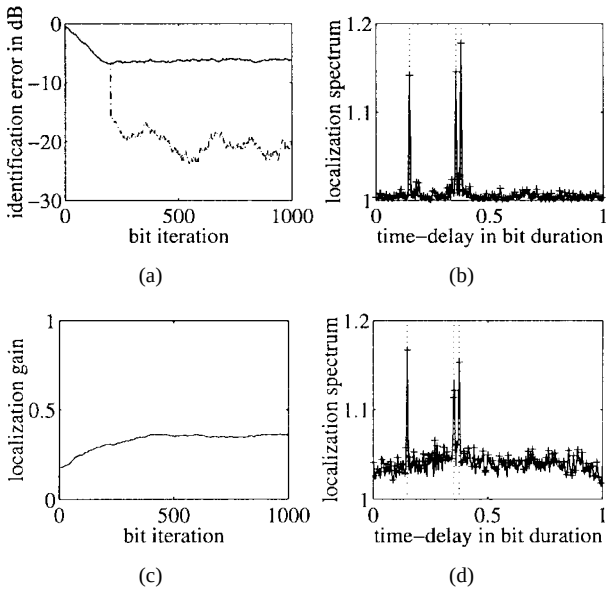

Fig. 3. $\sigma_I^2 = 64$ and Doppler of 1.76 Hz. (a) Identification error in dB without spatio-temporal reconstruction (solid) and with tracking (semi-dashed). (b) Localization spectrum (solid) and its root solutions (''+'') using STAR-SS. (c) Localization gain. (d) Localization spectrum (solid) and its root solutions (''+'') using STAR-ES.

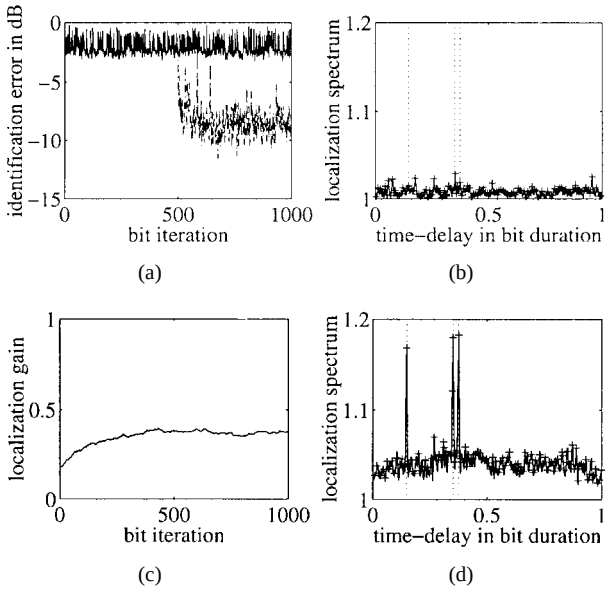

Fig. 4. $\sigma_I^2 = 64$ and Doppler of 440 Hz. (a) Identification error in dB without spatio-temporal reconstruction (solid) and with tracking (semidashed). (b) Localization spectrum (solid) and its root solutions (''+'') using STAR-SS. (c) Localization gain. (d) Localization spectrum (solid) and its root solutions (''+'') using STAR-ES.

V. Simulation Results

A. Localization (i.e., Synchronization) Results

We rely on simulations to illustrate the performance of STAR under difficult localization and tracking conditions. For the evaluation of multipath localization with STAR, we consider the configuration of $M = 4$ sensors, $P = 3$ paths with constant time-delays $\tau_1 \simeq 0.15T$, $\tau_2 \simeq 0.35T$, and $\tau_3 \simeq 0.38T$, a maximum number of resolvable paths $P_{\max} = 5$, and a processing gain $L = 128$. We use Jakes' model [32] of Rayleigh fading to generate propagation data. We generate two sets of $M \times P = 12$ uncorrelated Rayleigh fading paths at the data bit rate of 9.6 kb/s, with Dopplers of almost 1.76 Hz and 440 Hz, respectively. Perfect power control is assumed (see power control capacity in [19]) where the total received power is $\psi^2(t) = 1$. The power is assumed to be equally distributed over the three paths[11] (i.e., $\varepsilon_{p,n}^2 = 1/3$). The estimate of the total received power $\hat{\psi}_0^2$ is initialized at 0.1, and $\hat{\underline{\mathrm{H}}}_0$ in (10), with norm $\sqrt{M}$ as well as $\hat{\mathbf{U}}_0$ in (15), with columns normalized to 1 are started with random values. The smoothing factor α is always set to 0.01 in (9).

In the first scenario, the interference $I(t)$ in (1) has $\sigma_I^2 = 64$ (i.e., $\mathrm{SINR_{in}} \simeq -18$ dB, or 3 dB after despreading) and the Doppler is 1.76 Hz. We fix $\mu = 0.02$ and $\eta = 0.005$ in (10) and (15), respectively. In Fig. 3(a), identification errors $|1 \pm \tilde{\underline{\mathrm{H}}}_n^H \underline{\mathrm{H}}_n/M|^2$ (solid line) show that $\tilde{\underline{\mathrm{H}}}_n$ converges rapidly to the spatio-temporal channel within about $200T$. In Fig. 3(b), the localization spectrum of STAR-SS and its root solutions, given after convergence, provide estimates of the number of paths and their time-delays with an accuracy of roughly $10^{-3}T$.

[11] It should be understood, however, that Rayleigh fading variations are still present in the elements of propagation vectors $G_{p,n}$, despite normalization. We select such an idealistic power fractions profile to allow the evaluation of the detection of appearing or disappearing multipaths (see Section V-B).

The spatio-temporal reconstruction from these estimates at $n = 200$ and the multipath tracking reduce identification errors $|1 \pm \hat{\underline{\mathrm{H}}}_n^H \underline{\mathrm{H}}_n/M|^2$ by almost $10 \log_{10}(L/P) \simeq 16$ dB as expected [see Fig. 3(a), semidashed line], and decrease the bit error rate (BER) in the considered scenario by almost a factor of 50 down to 10^{-3}. In Fig. 3(c), the localization gain $(\mathrm{tr}(\mathbf{D}^H \hat{\mathbf{U}}_n \hat{\mathbf{U}}_n^H \mathbf{D})/MP)^{1/2}$ shows that STAR-ES converges at a slower rate, within about $400T$. Its localization spectrum and its root solutions, in Fig. 3(d), show a performance in localization comparable to STAR-SS. Notice here that the double root solution of the second path is merged into a single time-delay using a rule similar to (31). Despite the high resolution capacity of STAR-ES, the noise present in the signal eigensubspace, as well as the low Doppler, slow down its convergence and reduce its performance. In such a case it is better to use STAR-SS, whose complexity is lower.

In the second scenario, we increase the Doppler to 440 Hz and fix $\mu = 0.5$ and $\eta = 0.01$. In Fig. 4(a), identification errors (solid line) show that $\tilde{\underline{\mathrm{H}}}_n$ fails to track the very high variations of the spatio-temporal channel. In Fig. 4(b), the localization spectrum of STAR-SS and its root solutions, estimated at $n = 500$, reveal none of the time-delays. The advantages of STAR-ES over STAR-SS are evident here. Fig. 4(c) shows that STAR-ES still converges within $400T$, despite the presence of a fast Doppler. Its localization spectrum and its root solutions, in Fig. 4(d), show a performance comparable to the previous scenario. The spatio-temporal reconstruction from the resulting time-delay estimates is made at $n = 500$ using $\mathbf{Z}_n$ instead of $\tilde{\mathbf{H}}_n$ in (18). The multipath tracking, following this step, again reduces identification errors as shown in semi-dashed line of Fig. 4(a), but the misadjustment increases with a faster Doppler.

In the third example, we decrease the interference power to $\sigma_I^2 = 16$ (i.e., $\mathrm{SINR_{in}} \simeq -12$ dB, or 9 dB after despreading)

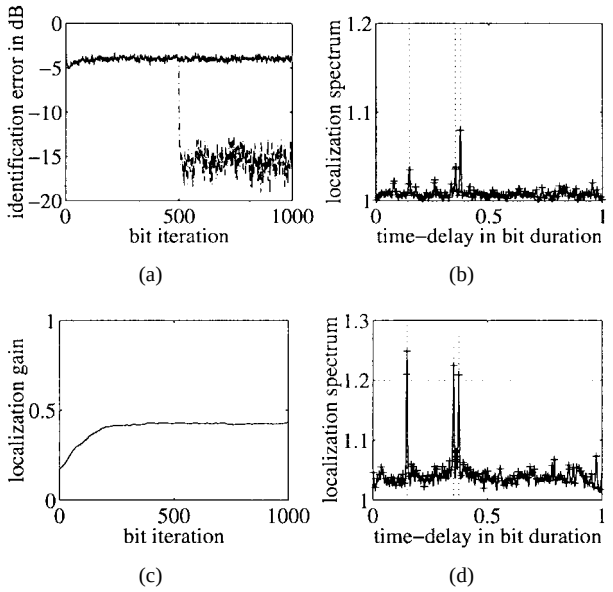

Fig. 5. $\sigma_I^2 = 16$ and Doppler of 440 Hz. (a) Identification error in dB without spatio-temporal reconstruction (solid) and with tracking (semi-dashed). (b) Localization spectrum (solid) and its root solutions (''+'') using STAR-SS. (c) Localization gain. (d) Localization spectrum (solid) and its root solutions (''+'') using STAR-ES.

TABLE I

	application	convergence	complexity	accuracy
STAR-SS	slow Doppler	fast	$O(ML)$	fair
STAR-ES	fast Doppler	slow	$O(MP_{\max}L)$	high resolution

and fix $\mu = 0.5$ and $\eta = 0.01$. In Fig. 5(a), the spatio-temporal identification is seen to converge rapidly, but the misadjustment is higher (solid line) than in Fig. 3(a). In Fig. 5(b), the localization spectrum of STAR-SS and its root solutions almost reveal the time-delays, but the estimation with STAR-SS is not reliable in the presence of a fast Doppler, even at a lower interference level. On the other hand, Fig. 5(c) shows that STAR-ES has a better convergence behavior. Its performance in localization improves significantly, as illustrated by the localization spectrum and its root solutions of Fig. 5(d). The spatio-temporal reconstruction is again made at $n = 500$, this time using $\hat{\mathbf{H}}_n$ in (18) as usually defined. Again, multipath tracking reduces the identification errors as shown by the semi-dashed line of Fig. 5(a). Compared to Fig 4(a), the misadjustment is seen to decrease with lower interference.

Table I compares the relevant performance features of STAR-SS and STAR-ES.[12]

B. Tracking Results

For the evaluation of multipath time-delay tracking with STAR, we consider the same configuration and the three different conditions discussed above. However, the multipath time-delays are no longer constant, but vary in time along the trajectories of Fig. 6(a). We further assume that the first path vanishes at $n = 4000T$ and reappears at $n = 7000T$,

[12]The complexity is given here for the temporary stage of localization. It excludes the permanent tracking step whose dominant term is of $O(MPL)$.

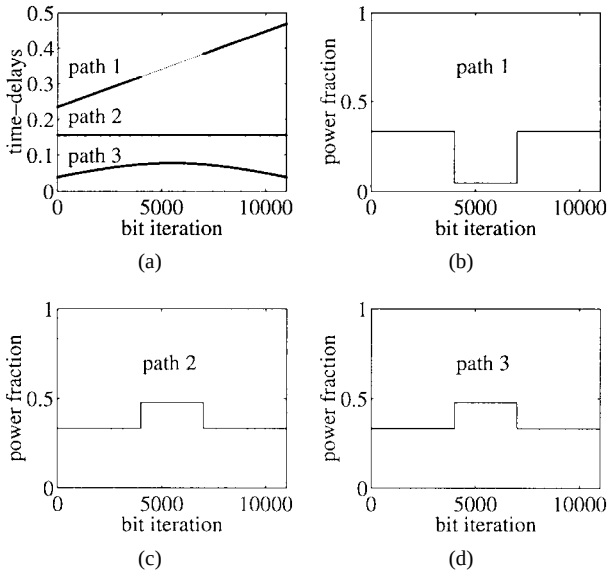

Fig. 6. (a) True time-delays $\tau_{p,\,n}$. (b)–(d) True power fractions $\varepsilon_{p,\,n}^2$.

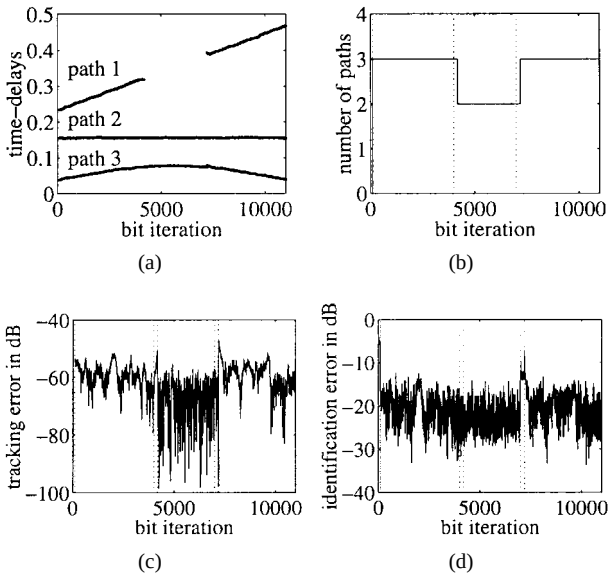

Fig. 7. $\sigma_I^2 = 64$ and Doppler of 1.76 Hz. (a) Estimated time-delays $\hat{\tau}_{p,\,n}$. (b) Estimated number of paths $\hat{P}$ (solid). (c) Time-delay tracking error $\sum_{p=1}^{\hat{P}} |\tau_{p,n} - \hat{\tau}_{p,n}|^2/\hat{P}$. (d) Identification error $|1 \pm \underline{\hat{\mathrm{H}}}_n^H \underline{\mathrm{H}}_n/M|^2$ in dB.

as shown in Fig. 7(b). Therefore, the power fractions of the second and third paths in Fig. 6(c) and (d) increase equally during that time interval to guarantee both $\sum_{p=1}^{P} \varepsilon_p^2(t) = 1$ and $\psi^2(t) = 1$ (i.e., perfect power control situation).

In the first scenario corresponding to Fig. 3 (i.e., $\sigma_I^2 = 64$ and Doppler of 1.76 Hz), we initialize STAR with the source-structure localization option STAR-SS and start time-delay tracking within $100T$, even before steady state convergence is reached. We fix $\mu = 0.1$ and $\xi = 0.3$ in (23) and (26), respectively. In Fig. 7(a), we see that the time-delays are properly tracked despite the disappearance and appearance of the first path. Indeed, Fig. 7(b) shows that the number of paths is correctly estimated. The disappearance and reappearance of the first path are rapidly detected with estimation delays less than $100T$. In Fig. 7(c), we plot the time-delay tracking error

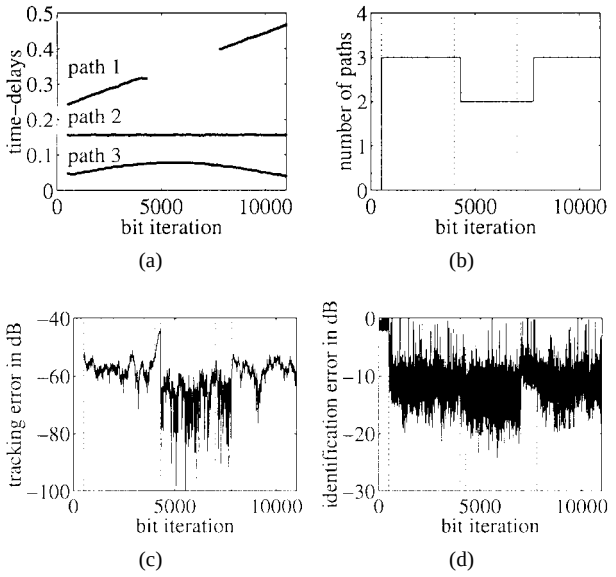

Fig. 8. $\sigma_I^2 = 64$ and Doppler of 440 Hz. (a) Estimated time-delays $\hat{\tau}_{p,n}$. (b) Estimated number of paths $\hat{P}$ (solid). (c) Time-delay tracking error $\sum_{p=1}^{\hat{P}} |\tau_{p,n} - \hat{\tau}_{p,n}|^2/\hat{P}$. (d) Identification error $|1 \pm \hat{\underline{\mathrm{H}}}_n^H \underline{\mathrm{H}}_n/M|^2$ in dB.

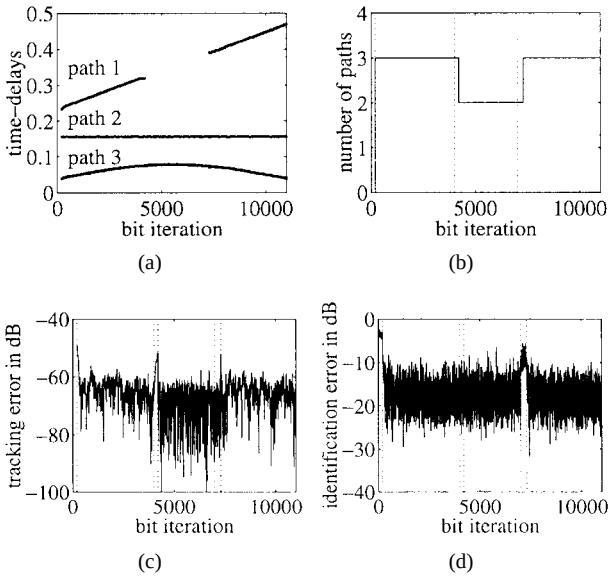

Fig. 9. $\sigma_I^2 = 16$ and Doppler of 440 Hz. (a) Estimated time-delays $\hat{\tau}_{p,n}$. (b) Estimated number of paths $\hat{P}$ (solid). (c) Time-delay tracking error $\sum_{p=1}^{\hat{P}} |\tau_{p,n} - \hat{\tau}_{p,n}|^2/\hat{P}$. (d) Identification error $|1 \pm \hat{\underline{\mathrm{H}}}_n^H \underline{\mathrm{H}}_n/M|^2$ in dB.

$\sum_{p=1}^{\hat{P}} |\tau_{p,n} - \hat{\tau}_{p,n}|^2/\hat{P}$ and show that absolute errors are as small as $10^{-3}T$. Channel identification errors are also reduced below -20 dB, as shown in Fig. 7(d). Notice, in Fig. 7(c), that tracking refines localization results at initialization or at the restart of STAR. When the first path vanishes without completely disappearing, STAR stops tracking it and tracking errors increase for a short interval until this event is detected. The energy component of the first path becomes negligible [see (30)] and has practically no effect on the identification errors of Fig. 7(d). When the first path reappears, identification errors increase for a short interval until this event is detected. Notice, however, that the identification errors have no effect on the tracking process, which can be seen in Fig. 7(c) to be robust to abrupt changes in multipath number and power distribution. The tracking errors decrease slightly with fewer multipaths since each resolvable path component carries a greater fraction of the total received power[13] [see Fig. 6(c) and (d)].

In the second example, corresponding to Fig. 4, we increase the Doppler to 440 Hz and fix $\mu = 0.6$ and $\xi = 0.4$. We observe in Fig. 8 that STAR performs nearly as well in the presence of very fast Doppler. However, the initialization or restart of STAR is slower than in Fig. 7 and requires almost $500T$ with STAR-ES. The detection of the vanishing path is also slower and requires almost $200T$. The tracking errors remain in the same range but the identification errors show a higher misadjustment, close to -10 dB.

In the third scenario corresponding to Fig. 5, this time we reduce the interference power to $\sigma_I^2 = 16$ and fix $\mu = 0.5$ and $\xi = 0.3$. We observe, in Fig. 9, that STAR tracks faster with lower interference. The initialization and restart with STAR-ES require almost $200T$, while the detection of the vanishing path requires almost $100T$. The misadjustment of identification errors also improves to almost -15 dB. However, tracking errors again remain in the same range of $10^{-3}T$. Overall, the results reveal a tracking behavior for STAR that is very robust to different levels of interference and Doppler.

[13] Notice that the configuration is different from [14] where a perfect power control situation is not considered and where the loss in received power is compensated by power control when the first path vanishes.

VI. Conclusions

The spatio-temporal array-receiver (STAR) we proposed for asynchronous cellular CDMA offers many advantages when compared to previous methods [3]–[9].

- *Attractive Formulation:* STAR derives from the block despread data an attractive instantaneous mixture model of a narrowband source with a one-dimensional spatio-temporal channel and processes it at the bit rate. This model called PCM allows for a structural approach to blind channel equalization and time-delays acquisition. It enables the application of efficient narrowband signal processing techniques based on an STS approach of the channel where multipath time-delay estimation can be particularly treated by DOA localization and tracking techniques.
- *Very Low Complexity:* STAR has a very simple structure of narrowband processors, and requires only $O(ML)$ and $O(MP_{\max}L)$ operations per bit for temporary localization with STAR-SS and STAR-ES, respectively, and $O(MPL)$ for permanent tracking.
- *High Performance:* STAR manifests fast and accurate time-delays acquisition and tracking in the presence of strong interference and very fast Doppler. It adapts readily to newly appearing or disappearing paths. These properties are essential for high performance in asynchronous cellular CDMA. It also optimally reduces interference by DFI and can potentially accommodate a larger number of users per cell [19].

REFERENCES

[1] S. C. Swales, M. A. Beach, D. J. Edwards, and J. P. McGreehan, "The performance enhancement of multibeam adaptive base-station antennas for cellular land mobile radio systems," *IEEE Trans. Veh. Technol.*, vol. 39, pp. 56–67, Feb. 1990.

[2] J. H. Winters, J. Salz, and R. D. Giltin, "The impact of antenna diversity on the capacity of wireless communication systems," *IEEE Trans. Commun.*, vol. 42, pp. 1740–1751, Feb.–Apr. 1994.

[3] A. J. Viterbi, *CDMA Principles of Spread Spectrum Communication.* Reading MA: Addison-Wesley, 1995.

[4] A. Jalali and P. Mermelstein, "Effects of diversity, power control, and bandwidth on the capacity of microcellular CDMA systems," *IEEE J. Select. Areas Commun.*, vol. 12, pp. 952–961, June 1994.

[5] A. F. Naguib and A. Paulraj, "Effects of multipath and base-station antenna arrays on uplink capacity of cellular CDMA," in *Proc. GLOBECOM'94*, 1994, pp. 395–399.

[6] J. R. Fonollosa, J. A. R. Fonollosa, Z. Zvonar, and J. Vidal, "Blind multiuser identification and detection in CDMA systems," in *Proc. ICASSP'95*, 1995, vol. III, pp. 1876–1879.

[7] O. M. Medina and J. F. Rubio, "Blind multi-user combining at the base-station for asynchronous CDMA systems," in *Proc. ICASSP'96*, 1996, vol. 5, pp. 2710–2713.

[8] A. J. Paulraj and C. B. Papadias, "Space-time signal processing for wireless communications," *IEEE Signal Processing Mag.*, vol. 14, pp. 49–83, Nov. 1997.

[9] H. Liu and G. Xu, "Blind equalization for CDMA systems with aperiodic spreading sequences," in *Proc. ICASSP'96*, 1996, vol. 5, pp. 2658–2661.

[10] L. Dumont, M. Fattouche, and G. Morrison, "Super-resolution of multipath channels in a spread spectrum location system," *IEE Electron. Lett.*, vol. 30, no. 19, pp. 1583–1584, Sept. 1994.

[11] M. D. Zoltowski and J. Ramos, "Blind multi-user access interference cancellation for CDMA based PCS/cellular using antenna arrays," in *Proc. ICASSP'96*, 1996, vol. 5, pp. 2730–2733.

[12] J. Ramos, M. D. Zoltowski, and H. Liu, "A low-complexity space-time processor for DS-CDMA communications," *IEEE Signal Processing Lett.*, vol. 4, pp. 259–261, Sept. 1997.

[13] S. Affes and P. Mermelstein, "Space/time multipath separation and equalization in asynchronous CDMA using the spatio-temporal array-receiver," in *Proc. ICUPC'97*, 1997, vol. 2, pp. 510–515.

[14] ———, "Spatio-temporal array-receiver for multipath tracking in cellular CDMA," in *Proc. ICC'97*, 1997, vol. 3, pp. 1340–1345.

[15] J. Gunther and A. Swindlehurst, "Algorithms for blind equalization with multiple antennas based on frequency domain subspaces," in *Proc. ICASSP'96*, 1996, vol. 5, pp. 2421–2424.

[16] M. Wax and A. Leshem, "Joint estimation of time delays and directions of arrival of multiple reflections of a known signal," in *Proc. ICASSP'96*, 1996, vol. 5, pp. 2622–2625.

[17] M. Vanderveen, C. Papadias, and A. Paulraj, "Joint angle and delay estimation (JADE) for multipath signals arriving at an antenna array," *IEEE Commun. Lett.*, vol. 1, pp. 12–14, Jan. 1997.

[18] A.-J. van der Veen, M. Vanderveen, and A. Paulraj, "SI-JADE: An algorithm for joint angle and delay estimation using shift-invariance properties," in *Proc. SPAWC'97*, 1997, pp. 161–164.

[19] S. Affes and P. Mermelstein, "Capacity improvement of cellular CDMA by the subspace-tracking array-receiver," in *Proc. SPAWC'97*, 1997, pp. 233–236.

[20] S. Affes, S. Gazor, and Y. Grenier, "A subarray manifold revealing projection for partially blind identification and beamforming," *IEEE Signal Processing Lett.*, vol. 3, pp. 187–189, June 1996.

[21] ———, "An algorithm for multisource beamforming and multitarget tracking," *IEEE Trans. Signal Processing*, vol. 44, pp. 1512–1522, June 1996.

[22] ———, "An algorithm for multi-source beamforming and multi-target tracking: Further results," in *Proc. EURASIP EUSIPCO'96*, 1996, vol. I, pp. 543–546.

[23] S. U. Pillai, *Array Signal Processing.* New York: Springer-Verlag, 1989.

[24] G. Bienvenu and L. Kopp, "Optimality of high resolution array processing using the eigensystem approach," *IEEE Trans. Acoustics, Speech, Signal Processing*, vol. 31, pp. 1235–1247, Oct. 1983.

[25] R. O. Schmidt, "Multiple emitter location and signal parameter estimation," *IEEE Trans. Antennas Propagat.*, vol. 34, pp. 276–280, Mar. 1986.

[26] A. J. Barabell, "Improving the resolution performance of eigenstructure-based direction-finding algorithms," in *Proc. ICASSP'83*, 1983, vol. 1, pp. 336–339.

[27] Y. Bresler and A. Macovski, "Exact maximum likelihood parameter estimation of superimposed exponential signals in noise," *IEEE Trans. Acoustics, Speech, Signal Processing*, vol. 34, pp. 1081–1089, Oct. 1986.

[28] I. Ziskind and M. Wax, "Maximum likelihood localization of multiple sources by alternating projection," *IEEE Trans. Acoustics, Speech and Signal Processing*, vol. 34, pp. 1553–1560, Oct. 1988.

[29] R. Roy and T. Kailath, "ESPRIT—Estimation of signal parameters via rotational invariance techniques," *IEEE Trans. Acoustics, Speech and Signal Processing*, vol. 37, pp. 984–995, July 1989.

[30] B. Yang, "Projection approximation subspace tracking," *IEEE Trans. Signal Processing*, vol. 43, pp. 95–107, Jan. 1995.

[31] C. Riou and T. Chonavel, "Fast adaptive eigenvalue decomposition: A maximum likelihood approach," in *Proc. ICASSP'97*, 1997, vol. 5, pp. 3565–3568.

[32] W. C. Jakes, Ed., *Microwave Mobile Communications.* New York: John Wiley, 1974.

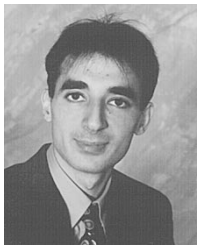

Sofiène Affes (S'94–M'95) was born in Tunisia in 1969. He received the Diplôme d'Ingénieur degree in electrical engineering and the Ph.D. degree in signal and image processing from the École Nationale Supérieure des Télécommunications, Paris, France in 1992 and 1995, respectively.

In 1991, he was a Visiting Scholar at the Cambridge University Engineering Department, Cambridge, U.K., where he worked on speech recognition. From 1995 until 1997, he was with INRS-Telecommunications at the University of Quebec, Verdun, Quebec, Canada, as a Research Associate, working on wireless CDMA systems. Currently, he is an Assistant Professor in the Personal Communications Group at INRS-Telecommunications. His research interests are in statistical signal and array processing with applications to wireless communications, acoustics and speech processing. He was involved in the European ESPRIT projects, 2101 ARS during 1991 and in 6166 FREETEL from 1993 to 1994, and currently contributes to the program of the Bell Quebec/NORTEL/NSERC Industrial Research Chair in Personal Communications.

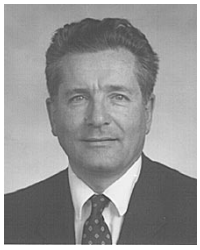

Paul Mermelstein (S'58–M'63–SM'77–F'94) received the B.Eng. degree in engineering physics from McGill University, Montreal, Canada, in 1959, and the S.M.E.E., and D.Sc. degrees in electrical engineering from the Massachusetts Institute of Technology, Cambridge, in 1960, 1963, and 1964, respectively.

From 1964 to 1973, he was a Member of Technical Staff in the Speech and Communications Research Department of Bell Laboratories, Murray Hill, NJ. From 1973 to 1977, he was a member of the Research Staff at Haskins Laboratories, conducting research in speech analysis, perception, and recognition. From 1977 to 1994, he was with Bell Northern Research, in a variety of management positions, leading research and development activities in speech recognition, speech coding, and personal communications. Currently, he is the holder of the Bell Quebec/NORTEL/NSERC Industrial Research Chair in Personal Communications at INRS-Telecommunications, University of Quebec, Verdun, and Auxiliary Professor of Electrical Engineering at McGill University. He is a leader of the major program in personal and mobile communications of the Canadian Institute for Telecommunications Research.

He is a past Associate Editor for Speech Processing of the *Journal of the Acoustical Society of America* and Editor for Speech Communications of the IEEE TRANSACTIONS ON COMMUNICATIONS.